The 2010 IEEE/RSJ International Conference on
Intelligent Robots and Systems
October 18-22, 2010, Taipei, Taiwan

Dynamic Obstacle Crossing by a Biped Robot, Based on Control of the Propulsion Energy

Paul-François Doubliez, Olivier Bruneau, Fethi Ben Ouezdou, *Member, IEEE*

Abstract— This paper proposes an energy control method for the dynamic walking of a planar biped, allowing obstacle crossing. This approach was tested in simulation on a numerical model of the HYDROÏD robot of the Laboratoire d'Ingénierie des Systèmes de Versailles, and achieved a dynamic walking with a 1.3 m/s maximum speed and the crossing of an obstacle thanks to inertia forces, by leaning with the front foot on the obstacle. The propulsion energy of the system is produced by the rear leg, endowed with four actuated degrees-of-freedom (hip, knee, ankle, toes), and controlled by a force control using four degrees-of-freedom in the non singular case, and three degrees-of-freedom in the singular case.

I. INTRODUCTION

The most performant humanoid robots concerning the walking are currently PETMAN, ASIMO [1], QRIO [2], HRP-2 [3], KHR-3 (HUBO) [4], WABIAN-2LL [5], WABIAN-2 [6] , BHR-02 [7], JOHNNIE [8], LUCY [9]. These robots move preferably on flat and structured (regular slopes, stairs) terrain and most of them have a very low speed compared to the human one. Nevertheless, in comparison with a wheeled vehicle, one of the main advantages of a walking machine lies in its capacity to cross some obstacles with various shapes and sizes in a non-structured environment. To meet this objective, it is necessary to develop some algorithms for the dynamic obstacle crossing for biped systems. It is worth noting that we define the « dynamic crossing » term by the crossing of an obstacle, leaning on it and using the system inertia in order to surmount it. Although this kind of motion seems simple and natural for human beings, its achievement in the robotics field presents a real challenge.

Indeed, how could we control our robot so that it crosses the obstacle without falling, i.e. so that its energy would neither be too low, in which case it would risk falling backwards, nor too high, which would induce an uncontrolled forwards fall?

The papers about dynamic obstacle crossing of non negligible size are scarce. We can cite Sabourin [10] who started to investigate this issue in the case of an obstacle of low height (15 mm) and with point contacts between the feet and the ground. Furthermore, the energy contribution for the dynamic walking and for the dynamic obstacle crossing needs to be discussed, because during the walking many ways to inject energy exist: thanks to the propulsion of the rear leg in double support phase and at the end of the stance phase, the hip traction during the stance phase, the inclination and the acceleration of the torso, the leg transfer and also to the twisting motion of the pelvis, etc… In order to succeed in crossing a relatively high obstacle, for example a rock or a low wall, amongst the energetic inputs indicated above, the propulsion in double support phase by the rear leg with active toes is predominant.

So as to generate the energy, according to the theorem of energy conservation, we will propose a force control of the rear leg, servoed on the total mechanical energy to provide, with four degrees-of-freedom (hip, knee, ankle, and toes) or with three degrees-of-freedom (hip, ankle and toes) in the singular case when the rear leg is stretched. A continuous transition from the first system to the second will also be proposed.

Firstly we briefly introduce a modelling of the HYDROÏD robot used to test the obstacle crossing, and then we explain the control method and its integration in a global walking control strategy. Lastly, results are presented, concerning forces, velocity and motor torques so as to size the sagittal actuators of HYDROÏD.

II. MODELLING

In order to test the energy control, a planar simulator inspired by HYDROÏD robot designed at LISV [11][12] was developed using ADAMS software for simulating the dynamical behaviour of multi-body systems. The kinematic structure of the simulator involves nine rotational joints with axes normal to the sagittal plane of the robot: one rotational joint between the pelvis and the torso, and four revolute joints in each leg (hip, knee, ankle, toes). The robot mass is about 70 kg. The leg masses are negligible compared with the masses of the pelvis and of the torso.

III. PROPULSION BY CONTROL OF PROPULSION ENERGY

A. Assumption of energy conservation during the stance phase and total mechanical energy target

The control that we now introduce is based on the assumption of mechanical energy conservation during the stance phase.

We consider that during this phase the HYDROÏD robot, endowed with four active degrees-of-freedom per leg (hip, knee, ankle, toes) and with two masses of 30 kg each one concentrated at the pelvis and at the torso extremity, can be

P. F. Doubliez is with LISV System Engineering Laboratory of UVSQ Versailles Saint-Quentin University, France (e-mail: doubliez@lisv.uvsq.fr)

O. Bruneau is with LISV System Engineering Laboratory of UVSQ Versailles Saint-Quentin University, France (phone: +33 139 254 762; e-mail: bruneau@lisv.uvsq.fr)

F. B. Ouezdou is with LISV System Engineering Laboratory of UVSQ Versailles Saint-Quentin University, France (e-mail: ouezdou@lisv.uvsq.fr)

modelled in the sagittal plane with a virtual inverse pendulum of constant length, with a concentrated mass in the middle of the torso segment, and having its rotation center at the ankle of the stance foot.

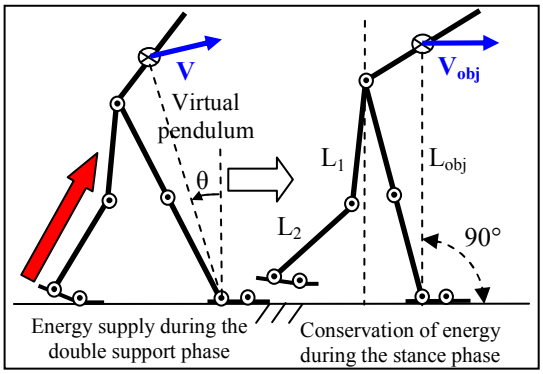

Fig 1 : double support and single support phases

This virtual pendulum has the following dynamic model:

$$\ddot{\theta} - \frac{g}{L_{obj}} \sin\theta = 0 \quad (1)$$

As illustrated in figure 1 simplifying HYDROÏD, if we want to reach a target altitude and speed of the virtual inverse pendulum when it is vertical, then using the assumption of energy conservation during the stance phase, it is possible to predict the amount of energy which should be supplied at the end of the double support phase, for example with a push of the rear leg. Thus we can write:

$$E^{Total}_{DoubleSupportEnd} = E^{Total}_{S\tan cePhaseObjective} \quad (2)$$

We wish to control the speed of the virtual inverse pendulum when this one is located at the top of its trajectory, named « objective position P^{obj} ». We consider that the top of the trajectory is reached when the inverse pendulum is in a vertical position. At the objective P^{obj}, the desired value of total mechanical energy of the virtual inverse pendulum is:

$$E^{T}_{obj} = \frac{1}{2} m.V^{2}_{obj} + m.g.L_{obj} \quad (3)$$

In figure 2, L_1, L_2 and L_3 are constant structural lengths. The θ_1^{obj} angle is the desired value of the inclination of the torso compared with the thigh. There might be a flexion θ_2^{obj} of the knee of the front leg, which we can take into account within the calculation of the « L_{obj} » distance. Indeed, in the case of a fast walking on flat terrain, this flexion of the front knee may remain small (less than 10 degrees), but it is no longer negligible during the dynamic crossing of the obstacle. The «d» distance in figure 2 locates the interval between the ankle joint (considered as center of rotation of the inverse pendulum) and the level of "zero reference" for the calculation of the potential energy.

Just before the "push phase" of the stance leg, the angles « θ_1^{obj} » and « θ_2^{obj} » are measured, and their desired values are frozen. We get « L_{obj} » as follows:

$$L_{obj} = d + H_{obj} \quad (4)$$

where « d » is the distance between the reference level for the calculation of the potential energy and the ankle rotation center, and therefore includes the height of the obstacle.

The « H^{obj} » distance is obtained with the following expression:

$$H_{obj} = \sqrt{L_1^2 + L_2^2 + L_3^2 + 2.L_1.L_2.\cos(\theta_2^{obj}) - 2.D_{obj}.L_3.\cos(\theta_1^{obj} + \theta_3^{obj})} \quad (5)$$

With:

$$D_{obj} = \sqrt{L_1^2 + L_2^2 + 2.L_1.L_2.\cos(\theta_2^{obj})} \quad (6)$$

$$\theta_3^{obj} = Arc\cos\left(\frac{L_1 + L_2.\cos(\theta_2^{obj})}{D_{obj}}\right) \quad (7)$$

Finally:

$$L_{obj} = d + \sqrt{a_1 - a_2} \quad (8)$$

With:

$$a_1 = L_1^2 + L_2^2 + L_3^2 + 2.L_1.L_2.\cos(\theta_2^{obj})$$

$$a_2 = 2.D^{obj}.L_3.\cos(\theta_1^{obj} + \theta_3^{obj})$$

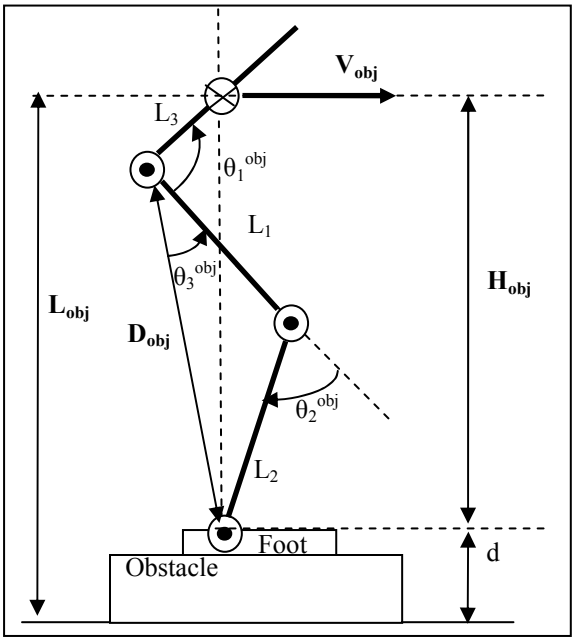

Fig 2 : configuration of segments of the robot at the target

B. Energy servo control of the propulsion force

In order to reach the energy target, we create a propulsion force to propel the robot, that we need to control in magnitude and in orientation, to supply the necessary propulsion energy in the right direction.

1) Control of the magnitude of the propulsion force

As we wish to reach a particular speed at a vertical position of the inverse pendulum, which is equivalent to reaching some level of total mechanical objective energy, the magnitude of the propulsion force during the double support phase (written « F_{prop} ») is computed by a proportional controller on the total energy E^T:

$$F_{prop} = k_{prop}.\left(E^{T}_{desired} - E^{T}_{mesured}\right) \quad (9)$$

By this means we achieve a high level « energy servo control » in order to propel the robot.
In practice, in the simulation, the « k_{prop} » gain was chosen with a value between 8 and 13 N/Joule for an established walking.We also employ a second important parameter during the propulsion phase: it is the angular threshold concerning the angle of the virtual inverse pendulum of the front leg, named « θ_{Stop} », from which the energy servo control is stopped. The crossing of this threshold constitutes a safety mechanism allowing the propulsion of the rear leg to be stopped, because it is possible that the total desired energy is overestimated compared with the size and the mass of the robot for example.

2) Control of the orientation of the propulsion force

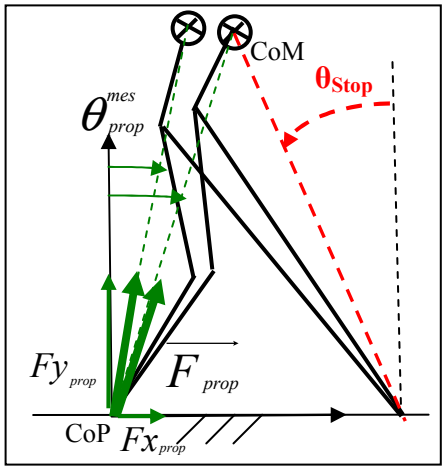

Fig 3 : orientation of the propulsion force

The orientation of the propulsion force is computed so that the force is always oriented towards the direction of the line defined by the pressure center of the rear foot (CoP) and the global system center of mass (CoM), located approximately equidistant from the masses of the pelvis and of the torso, as shown in figure 3. We write "θ_{prop}^{mes}" the measure of the inclination of the line (CoP-CoM), so we have:

$$Fx_{prop} = F_{prop}.\sin(\theta_{prop}^{mes}) \quad (10)$$

$$Fy_{prop} = F_{prop}.\cos(\theta_{prop}^{mes}) \quad (11)$$

C. Force control of the rear leg with two inverse kinematics

We wish to achieve some control supplying the propulsion energy via the rear leg in order to regulate the propulsion force. We will write the Jacobian matrix of a four-degrees-of-freedom leg, according to the parameters of figure 4, and by deriving the $\overrightarrow{O_1P}$ vector.

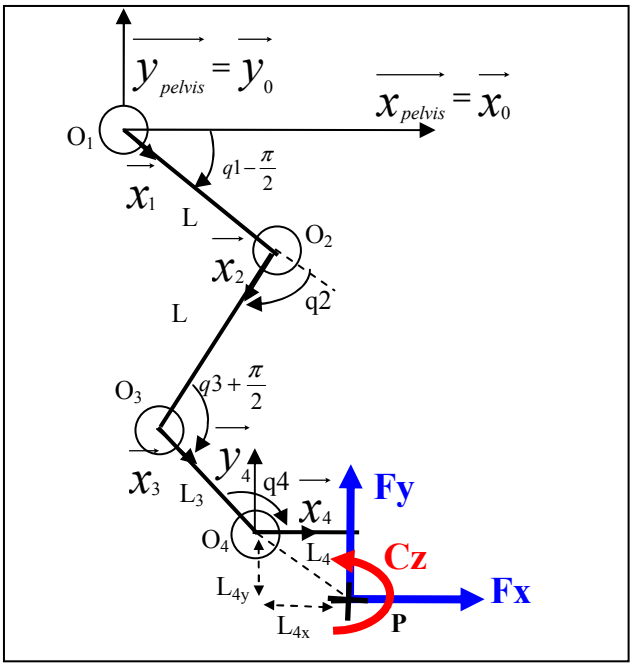

Fig 4 : notation for the writing of the inverse kinematics

The joints of the hip, the knee, the ankle and the toes are respectively located at points O_1, O_2, O_3 and O_4. The point P is a contact point of the toe with the ground, where the leg applies the vector of desired torque and forces (Cz, Fx, Fy). The lengths L_1, L_2, L_3 and L_4 are respectively the length of the thigh, the shinbone, the foot and from the center of rotation of the toe part to the P point. The model is setup under the following way:

$$\dot{X} = J.\dot{q} \quad \text{i.e.:} \begin{bmatrix} Wz \\ Vx \\ Vy \end{bmatrix} = J.\begin{bmatrix} \dot{q}1 \\ \dot{q}2 \\ \dot{q}3 \\ \dot{q}4 \end{bmatrix} \quad (12)$$

We write ci = cos(q_i) and si = sin(q_i), cij = cos(q_i+q_j) and sij = sin(q_i+q_j)… Dimension of the Jacobian matrix is 3x4:

$$J = \begin{pmatrix} J_{11} & J_{12} & J_{13} & J_{14} \\ J_{21} & J_{22} & J_{23} & J_{24} \\ J_{31} & J_{32} & J_{33} & J_{34} \end{pmatrix} (13)$$

With :

$J_{11} = 1$; $J_{12} = 1$; $J_{13} = 1$; $J_{14} = 1$

$J_{21} = L_1.c1 + L_2.c12 - L_3.s123 - L_{4x}.s1234 - L_{4y}.c1234$

$J_{22} = L_2.c12 - L_3.s123 - L_{4x}.s1234 - L_{4y}.c1234$

$J_{23} = -L_3.s123 - L_{4x}.s1234 - L_{4y}.c1234$

$J_{24} = -L_{4x}.s1234 - L_{4y}.c1234$

$J_{31} = L_1.s1 + L_2.s12 + L_3.c123 + L_{4x}.c1234 - L_{4y}.s1234$

$J_{32} = L_2.s12 + L_3.c123 + L_{4x}.c1234 - L_{4y}.s1234$

$J_{33} = L_3.c123 + L_{4x}.c1234 - L_{4y}.s1234$; $J_{34} = L_{4x}.c1234 - L_{4y}.s1234$

Using the Jacobian transposed, we get the model linking the joint torques and the propulsion forces applied at the point P, with the following form:

$$\tau = J^T.F \quad (14)$$

With :

$$\tau = \begin{bmatrix} \tau 1 \\ \tau 2 \\ \tau 3 \\ \tau 4 \end{bmatrix} (15) \text{ and } F = \begin{bmatrix} Cz \\ Fx \\ Fy \end{bmatrix} (16)$$

where «τ1», «τ2», «τ3» et «τ4» are respectively the joint torques of the hip, the knee, the ankle and the toes creating he propulsion force, and *F* is the vector of desired torque and forces in the operational workspace. In our case, the « Cz » desired value is equal to zero because we don't wish to create some torque from the leg on the ground, but only a propulsion force.

However, the inverse kinematics presented above is not convenient in the case where the rear leg is stretched, i.e. when the hip, knee and ankle joint centers are lined up. This kind of singular configuration of the subsystem {hip, knee and ankle} is quickly reached during the rear leg propulsion phase. Furthermore, by creating the propulsion force, the presented inverse kinematics has the disadvantage of performing non-anthropomorphic motions, for example by causing some hyper-extension of the rear knee, that is completely impossible for human beings.

That is why a second inverse kinematics was developed. In this second one, the knee joint is considered as locked on its articular limit, and the three torques hip, ankle, torques are computed in order to produce the propulsion force. In the case where the knee is locked, we have $dq_2/dt = 0$. It is worth noting that the q_2 angle is not necessarily equal to zero. With this second model, the Jacobian matrix of the inverse kinematics is a 3x3 dimension matrix:

$$J' = \begin{pmatrix} J_{11} & J_{13} & J_{14} \\ J_{21} & J_{23} & J_{24} \\ J_{31} & J_{33} & J_{34} \end{pmatrix} (17)$$

We get our inverse kinematics for the computation of the torques of the hip, the ankle and the toes:

$$\begin{bmatrix} \tau 1 \\ \tau 3 \\ \tau 4 \end{bmatrix} = J'^{T} \cdot \begin{bmatrix} Cz \\ Fx \\ Fy \end{bmatrix} (18)$$

This inverse kinematics is very useful to control the propulsion force if the three rotational joints hip, knee and ankle are lined up.

IV. GLOBAL CONTROL OF THE WALKING

The control of the walking is driven by a finite state machine partially printed on figure 5, for only one leg. We will now describe this finite state machine succinctly.

The simulation starts in the state « **initialization** » where the right foot is moved forward with a quasi stretched front leg, by bending the rear knee and toes.

Then, the robot enters the state of double support: « **L_Push** ». The left leg is torque-controlled thanks to equation (14) and then (18), in order to create the propulsion force with the high level energy servo control. The right stance leg ensures the horizontality of the pelvis with the hip joint, and the knee is locked in constant position so as to avoid leg bending. The end of this propulsion state is reached as soon as the inverse pendulum achieves the « θ_{Stop} » angle.

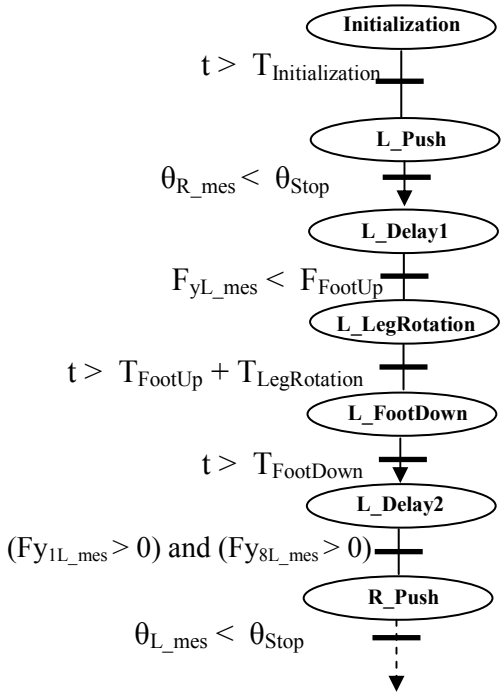

Fig 5 : state machine for a half step

In the « **L_Delay1** » state, the robot waits until the normal contact force comes below a threshold « F_{FootUp} », thanks to the inertia of the system generated by the propulsion force. Below this force threshold, the robot starts the swing leg transfer.

In the « **L_LegRotation** » state, the left foot is transferred, while the right stance leg maintains the horizontality of the pelvis, while locking the right knee. The right stance ankle turns passively, and reduces the energy consumption. The desired value of the left hip is built with an interpolation; boundary conditions allow satisfaction of the desired step length.

The next « **L_FootDown** » state, with a period of « $T_{FootDown}$ » allows bending of the thigh of the right rear leg, and stretching of the left leg before the contact with the ground. The right side hip continues to ensure the horizontal inclination of the pelvis.

In « **L_Delay2** », we are waiting for the contact of the left foot with the ground, and the impact is damped. After that, the exit transition of the « **L_Delay2** » state is reached, the machine enters the « **R_Push** » state, which is the beginning of a new half step, reversing the functions of the both legs.

V. RESULTS

We now present some results from the simulations done in ADAMS: some videos of a fast dynamic walking and of a dynamic walking with obstacle crossing are attached to this paper.

A. Fast dynamic walking

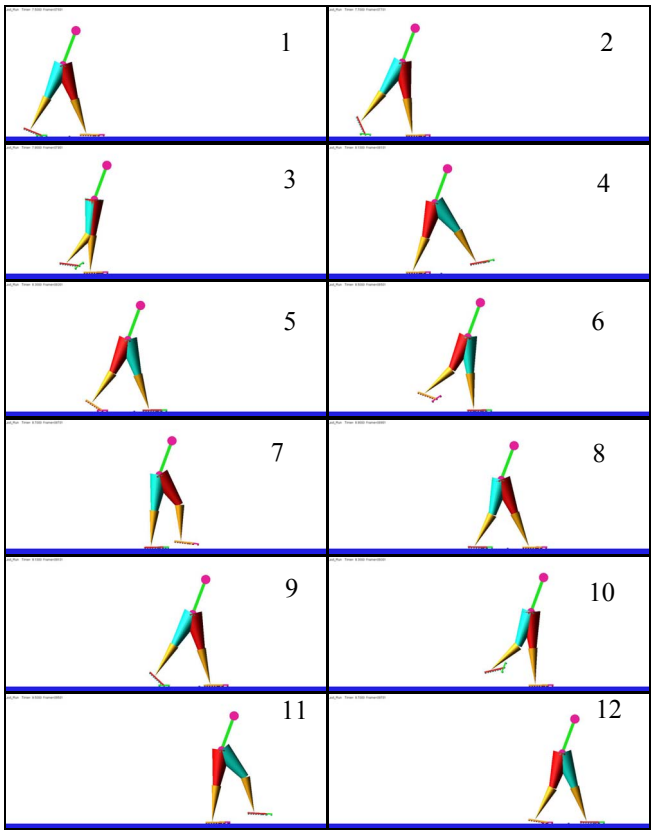

Fig 6 : 3 steps of dynamic walking, during 2.5 seconds

The small pictures of the figure 6 show an extract of fast dynamic walking, for a period of 2.5 seconds. Figure 7 indicates the achieved speed, with a velocity peak of 1.3 m/s and a mean speed of 0.8 m/s.

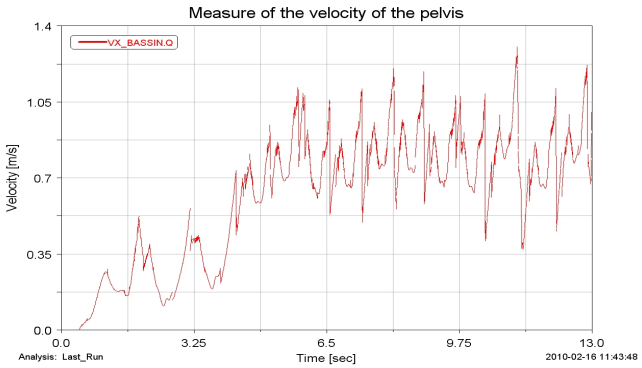

Fig 7 : pelvis velocity in the case of a fast walking

B. Dynamic walking with obstacle crossing

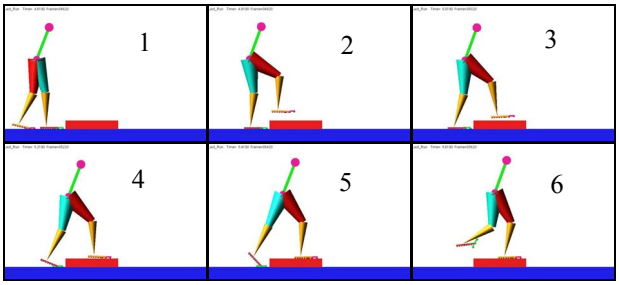

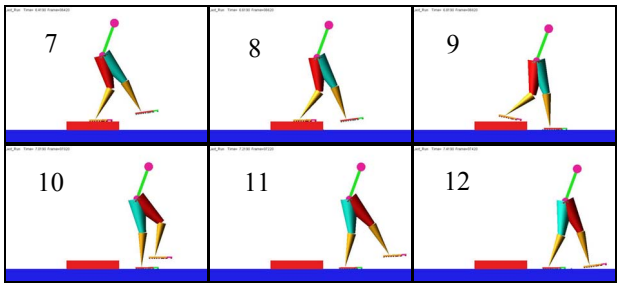

Fig 8 : dynamic obstacle crossing

The crossing of an obstacle of height 10 cm (approximately 9% of the total robot size) was simulated, as illustrated by the screenshots in figure 8.

C. Results curves at the obstacle crossing

1) Forward velocity

In figure 9, the horizontal velocity of the pelvis shows some significant decrease between 5 and 7.5 seconds, corresponding to the obstacle crossing, this causes some slowdown of the robot, but it does not stop it, because a new walking is subsequently established at a mean speed of approximately 0.6 m/s. The peak of 1.1 m/s stems from the descent of the obstacle: the robot is getting some additional kinetic energy.

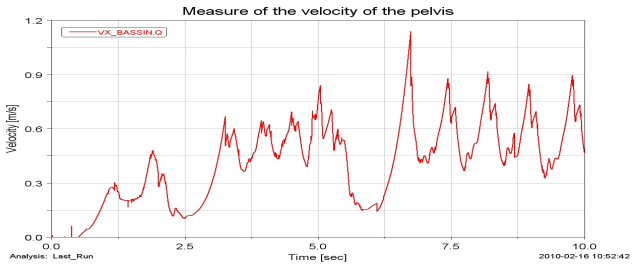

Fig 9 : measure of the pelvis velocity

2) Contact forces

It is also interesting to show the contact forces measured between the feet and the ground on figure 10.

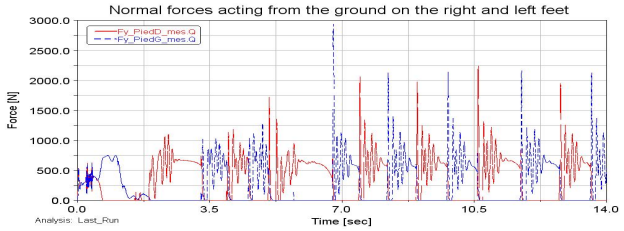

Fig 10: normal contact feet/ground forces

The obstacle crossing takes place between 5 and 6.7 seconds, in the stabilization area of the oscillations. Just before the 7th second, the highest impact peak arises from the landing of the foot on the ground, on stepping off the obstacle.

3) Actuator torques in the simulation of obstacle crossing

In order to design the actuators of the HYDROÏD robot, we need to examine the sagittal joint torques. We draw in figure

11 the four joint torques of the left rear leg, creating the propulsion force to climb onto a 10 cm obstacle.

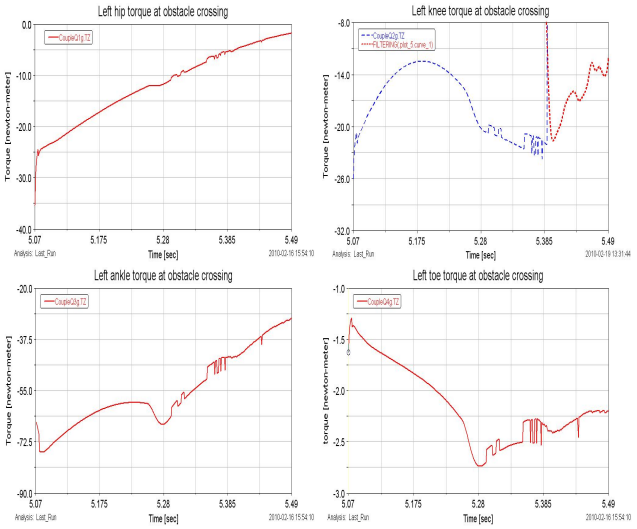

Fig 11 : the four actuators torques of the rear stance leg

We can notice that during the obstacle crossing, the ankle motor torque has the highest torque of all, with an absolute value of 76 Nm. The knee torque has a peak at 5.385 seconds, when the knee reaches the joint limitation: the rear leg is then almost fully stretched. The toe torque remains low (less than 3 Nm). Table 1 makes a comparison between the different maximum torques of the left leg (which produces the propulsion so as to overcome the obstacle), and the right leg in the case of a walking on a flat terrain.

joint	Left hip	Left knee	Left ankle	Left toe
|max torque| [Nm]	31	26	76	2.7
	Right hip	Right knee	Right ankle	Right toe
|max torque| [Nm]	39	25	57	1.4

Tab 1 : comparison between max torques

Finally, we can specify that during the stepping down from the obstacle, the robot has sufficiently kinetic energy for the propulsion force to be required for only a very short time (7 milliseconds).

VI. Conclusion and Future Work

Our high level energy control of the propulsion energy allowed us to achieve a fast dynamic walking with n steps, and our numerical model also succeeded to cross an obstacle. Our method, based on the total mechanical energy with a force control of the rear leg, will be further applied on HYDROÏD robot, thanks to the new actuator technology which will be installed on the prototype. Many possibilities for future works exist. We would like to apply the propulsion with the rear leg also during the stance phase, in the case of high speed, and to control explicitly the energy supply with some traction of the hip of the front leg during the crossing of the obstacle, in order to decrease the propulsion force. It will be necessary to adapt some parameters such as the « θ_{Stop} » angle or the « k_{prop} » gain of the energy controller, according to the desired speed of the robot. Lastly, this work sets up a preliminary phase before simulating a three-dimensional dynamic walking.

References

[1] Y. Sakagami, R. Watanabe, C. Aoyama, S. Matsunaga, N. Higaki and K. Fulimura. "The intelligent ASIMO, "system overview and integration" ", *Proceeding IEEE - International Workshop on Intelligent Robots & Systems (IROS)*, pp. 2478-2483, 2002.

[2] K. Nagasaka, Y. Kuroki, S. Suzuki, Y. Itoh, J. Yamaguchi, "Integrated motion control for walking, jumping and running on a small bipedal entertainment robot", *IEEE Proc. Of Int. Conf. On Robotics and Automation,* pp. 3189-3194, 2004.

[3] M. Stilman, K. Nishiwaki, S. Kagami, J. Kuffner, "Planning and Executing Navigation Among Movable Obstacles", *IEEE Proc. Of Int. Conf. On Intelligent Robots and Systems*, pp. 820-826, 2006.

[4] W. Park, J. Kim, J. Lee and J. Oh, "Online Free Walking Trajectory Generation for Biped Humanoid Robot KHR-3 (HUBO)", *IEEE Proc. Of Int. Conf. On Robotics and Automation*, pp. 1231-1236, 2006.

[5] Y. Ogura, T. Kataoka, H. Aikawa, H. Lim, A. Takanishi and K. Shimomura, "Evaluation of Various Walking Patterns of Biped Humanoid Robot", *IEEE Proc. Of Int. Conf. On Robotics and Automation*, pp. 603-608, 2005.

[6] M. Omer, Y. Ogura, H. Kondo, A. Morishima, G. Carbone, M. Ceccarelli, H. Lim, A. Takanishi, "Development of a humanoid robot having 2-DOF waist and 2-DOF trunk", *proceeding of 5th IEEE-RAS international conference*, pp. 333-338, 2005.

[7] J. Yang, Q. Huang, J. Li, C. Li, and K. Li, "Walking Pattern Generation for Humanoid Robot Considering Upper Body Motion", *IEEE Proc. Of Int. Conf. On Intelligent Robots and Systems*, pp. 4441-4446, 2006.

[8] S. Lohmeier, K. Löffler, M. Gienger, H. Ulbrich, F. Pfeiffer, "Computer system and control of biped Johnnie", *IEEE Proc. Of Int. Conf. On Robotics and Automation*, pp. 4222-4227, 2004.

[9] B. Vanderborght, B. Verrelst, R. Van Ham, M. Van Damme, P. Beyl, D. Lefeber, "Torque and Compliance Control of the Pneumatic Artificial Muscles in the Biped "Lucy" ", *IEEE Proc. Of Int. Conf. On Robotics and Automation*, pp. 842-847, 2006.

[10] C. Sabourin, O. Bruneau, "Robustness of the dynamic walk of a biped robot subjected to disturbing external forces by using CMAC neural networks", *Journal of Robotics and Autonomous Systems, Elsevier Science*, N°51, pp 81-99, 2005.

[11] S. Alfayad, F. B. Ouezdou, F. Namoun, O. Bruneau, P. Hénaff, "Three DOF Hybrid Mechanism for humanoid Robotic Application: Modeling, Design and Realisation". *IEEE Proc. Of Int. Conf. On Intelligent Robots and Systems*, pp. 4955-4961, 2009.

[12] S. Alfayad, F. B. Ouezdou, F. Namoun, "New Three DOF Ankle Mechanism for Humanoid Robotic Application: Modeling, Design and realization." *IEEE Proc. Of Int. Conf. On Intelligent Robots and Systems*, pp. 4969-4976, 2009.